Radiative susceptibility of cloudy atmospheres to droplet number perturbations: 1. Theoretical analysis and examples from MODIS

Steven Platnick[1] and Lazaros Oreopoulos[2]

Received 29 November 2007; revised 13 May 2008; accepted 21 May 2008; published 25 July 2008.

[1] Theoretical and satellite-based assessments of the sensitivity of broadband shortwave radiative fluxes in cloudy atmospheres to small perturbations in the cloud droplet number concentration (N) of liquid water clouds under constant water conditions are performed. Two approaches to study this sensitivity are adopted: absolute increases in N, for which the radiative response is referred to as "absolute cloud susceptibility," and relative increases in N or "relative cloud susceptibility." Estimating the former is more challenging as it requires an assumed value for either cloud liquid water content or geometrical thickness; both susceptibilities require an assumed relationship between the droplet volume and effective radius. Expanding upon previous susceptibility studies, present radiative calculations include the effect of ΔN perturbations on droplet asymmetry parameter and single-scattering albedo, in addition to extinction. Absolute cloud susceptibility has a strong nonlinear dependence on the droplet effective radius as expected, while relative cloud susceptibility is primarily dependent on optical thickness. Molecular absorption and reflecting surfaces both reduce the relative contribution of the cloud to the top-of-atmosphere (TOA) flux and therefore also reduce the TOA albedo susceptibility. Transmittance susceptibilities are negative with absolute values similar to albedo susceptibility, while atmospheric absorptance susceptibilities are about an order of magnitude smaller than albedo susceptibilities and can be either positive or negative. Observation-based susceptibility calculations are derived from MODIS pixel-level retrievals of liquid water cloud optical thickness, effective radius, and cloud top temperature; two data granule examples are shown. Susceptibility quantifies the aerosol indirect effect sensitivity in a way that can be easily computed from model fields. As such, susceptibilities derived from MODIS observations provide a higher-order test of model cloud properties used for indirect effect studies. MODIS-derived global distributions of cloud susceptibility and radiative forcing calculations are presented in a companion paper.

Citation: Platnick, S., and L. Oreopoulos (2008), Radiative susceptibility of cloudy atmospheres to droplet number perturbations: 1. Theoretical analysis and examples from MODIS, *J. Geophys. Res.*, *113*, D14S20, doi:10.1029/2007JD009654.

1. Introduction

[2] The global aerosol burden has substantially increased since the beginning of the industrialized era [*Intergovernmental Panel on Climate Change*, 2007]. Aerosol particles affect solar radiation by direct scattering and absorption, but can also change cloud properties through the subset of particles that act as cloud condensation nuclei (CCN) and ice nuclei (IN), a pathway referred to as the "indirect aerosol effect" (IAE). While the IAE is a continuum of effects and consequences, it is often considered the manifestation of two primarily different aerosol-cloud interaction mechanisms. One mechanism is the radiative effect due to cloud microphysical changes only (no change in cloud water or other properties). Here, the greater availability of CCN or IN yields clouds with more numerous but smaller cloud particles and therefore larger optical thicknesses (commonly referred to as the "Twomey effect" [*Twomey*, 1974] or 1st IAE). A second mechanism encompasses the effect of aerosols on cloud water, e.g., a decrease in cloud particle size decreasing precipitation efficiency and thereby increasing cloud lifetime, fraction [*Albrecht*, 1989], and/or physical thickness [*Pincus and Baker*, 1994]. This 2nd IAE can modify both cloud radiative and macrophysical properties. Clearly, the two mechanisms are coupled, but the separate partitioning is useful in understanding the relative role of each process for different cloud types and scenarios. Other microphysical consequences have been invoked for

[1]Laboratory for Atmospheres, NASA Goddard Space Flight Center, Greenbelt, Maryland, USA.
[2]Joint Center for Earth Systems Technology, University of Maryland, Baltimore County, Baltimore, Maryland, USA.

Copyright 2008 by the American Geophysical Union.
0148-0227/08/2007JD009654

convective clouds (e.g., effect on freezing level and dynamic development [*Khain et al.*, 2005]) while the non-microphysical "semi-indirect effect" of absorbing aerosol [*Hansen et al.*, 1997; *Ramanathan et al.*, 2001; *Koren et al.*, 2004] is thought to be an important modifier to cloud properties in some regimes and time periods.

[3] For liquid water clouds, recent theoretical studies of aerosol compositional effects and cloud microphysics [e.g., *Nenes et al.*, 2002] and Large Eddy Simulation (LES) cloud modeling studies with coupled aerosol-cloud microphysics [*Ackerman et al.*, 2004; *Xue and Feingold*, 2006; *Zuidema et al.*, 2008] have helped elucidate the details and subtleties of the IAE. However, satellite observational studies [*Sekiguchi et al.*, 2003; *Matsui et al.*, 2006] remain challenging because of the inherent difficulties involved in trying to quantify a partial derivative (i.e., a change in cloud properties due only to changes in aerosol amount and type, while all relevant dynamic/thermodynamic quantities remain fixed) from instantaneous measurements and incomplete cloud dynamic/thermodynamic information. Rather than confronting the formidable task of assessing this partial derivative of cloud properties in a particular place and time, we have adopted an alternative approach where satellite retrievals are used to estimate the cloud radiative sensitivity to a specified change in cloud droplet number concentration (N).

[4] The present study examines radiative flux sensitivities to droplet concentration perturbations in liquid water clouds under constant cloud water and geometrical thickness conditions. The sensitivity of reflected solar fluxes to N changes has been previously examined using the concept of "cloud susceptibility," a sensitivity parameter given by the change in cloud albedo for a differential change in N [*Platnick and Twomey*, 1994; *Taylor and McHaffie*, 1994; *Feingold et al.*, 1997; *Ackerman et al.*, 2000; *McFarquhar and Heymsfield*, 2001; *Chuang et al.*, 2002]. Here we broaden the study of susceptibility properties and dependencies to encompass the following: (1) relative as well as absolute changes in N, (2) perturbations in cloud droplet asymmetry parameter and single-scattering albedo (in addition to extinction), (3) transmittance and absorptance susceptibilities, and (4) broadband susceptibilities from operational Moderate Resolution Imaging Spectroradiometer (MODIS) cloud optical property retrievals along with retrieval-consistent broadband surface albedos and modeled atmospheric profiles.

[5] The ultimate goal is to obtain observation-based estimates of the indirect effect radiative forcing for specific cloud perturbation scenarios, given the current climate distribution of cloud properties. Global spatial and temporal distributions of the albedo sensitivity can be used to estimate the range of future radiative flux forcing responses, as well as provide an additional constraint on cloud properties in indirect effect modeling studies. A first step in this direction is investigated in a companion paper [*Oreopoulos and Platnick*, 2008, hereinafter referred to as Part 2] that examines the global and seasonal distribution of cloud susceptibility based on MODIS Level 3 (gridded) data.

[6] In section 2, we revisit the definition of cloud susceptibility and distinguish between absolute and relative susceptibilities. A discussion of the methodology and radiative transfer tools used to calculate susceptibility is given in section 3; example theoretical susceptibility results and dependencies are presented in section 4. The feasibility of observational-based susceptibility calculations is demonstrated in section 5 with MODIS data granules. Concluding comments on the utility of susceptibility are given in section 6.

2. Cloud Susceptibility

2.1. Absolute and Relative Cloud Albedo Susceptibility

[7] The sensitivity of cloud albedo to aerosol-induced perturbations in droplet number concentration, and the potential climatic consequences, were first discussed by *Twomey* [1974]. Cloud albedo susceptibility was later used to quantify and examine this sensitivity [*Twomey*, 1991; *Platnick and Twomey*, 1994]. It was defined as the change in cloud albedo (R) resulting from a differential change in N, with cloud water path and content held constant. The spectral susceptibility, S_λ, can be written as

$$S_\lambda = \frac{dR_\lambda(\tau_\lambda, \varpi_\lambda, g_\lambda)}{dN} = \frac{\partial R_\lambda}{\partial \tau_\lambda}\frac{d\tau_\lambda}{dr_e}\frac{dr_e}{dN} + \frac{\partial R_\lambda}{\partial \varpi_\lambda}\frac{d\varpi_\lambda}{dr_e}\frac{dr_e}{dN} + \frac{\partial R_\lambda}{\partial g_\lambda}\frac{dg_\lambda}{dr_e}\frac{dr_e}{dN}, \tag{1a}$$

where $r_e = \int r^3 n(r)dr \big/ \int r^2 n(r)dr$ is the effective radius of the droplet size distribution $n(r)$, τ_λ the cloud optical thickness, $\overline{\omega}_\lambda$ and g_λ the single-scattering albedo and asymmetry parameter of the droplet size distribution, respectively, and λ the wavelength. For both physical and practical reasons to be discussed later, it is also useful to look at albedo changes due to perturbations in the relative cloud droplet number concentration, i.e.,

$$S_\lambda^{rel} = \frac{dR_\lambda(\tau_\lambda, \overline{\omega}_\lambda, g_\lambda)}{\frac{dN}{N}} = NS_\lambda, \tag{1b}$$

which will be referred to as relative susceptibility. When distinguishing between the two forms is necessary, equation (1a) will be referred to as absolute susceptibility. While other susceptibility formulations involving relative perturbations in N are also useful, e.g., $dlnR_\lambda/dlnN$ [*Feingold and Seibert*, 2008], we chose equation (1b) because of our interest in absolute albedo perturbations for radiative forcing studies.

[8] Previous susceptibility studies considered only the first term in equation (1) which will be shown to be dominant later in this section. In that term, because

$$\tau_\lambda = \frac{3\overline{Q}_\lambda wH}{4\rho_l r_e} \tag{2}$$

for a vertically homogeneous cloud with geometrical thickness H, average spectral extinction efficiency of the droplet size distribution $\overline{Q}_\lambda$, and liquid water content w, then

$$\frac{d\tau_\lambda}{dr_e} = -\frac{\tau_\lambda}{r_e} \tag{3}$$

under constant cloud water path conditions. Common to all three terms in equation (1) is the derivative dr_e/dN, which can be expressed analytically as follows. The volume radius $r_v^3 = \int r^3 n(r)dr / \int n(r)dr$, water content, liquid water density

ρ_l, and N are related via $w = 4/3\ \rho_l \pi r_v^3 N$. With the assumption $r_v^3 \approx k r_e^3$ (k being a parameter ranging from ~0.6 to ~0.9 for marine stratocumulus [e.g., *Martin et al.*, 1994]), N is approximated by

$$N \approx \frac{3w}{4\pi\rho_l k r_e^3}. \tag{4}$$

For a constant water content and constant k process, equation (4) gives

$$\frac{dr_e}{dN} = -\frac{1}{3}\frac{r_e}{N}, \tag{5}$$

which is negative as expected. The susceptibility derivations and calculations that follow will use some form of both equations (3) and (5), and therefore assume that during a droplet perturbation process both cloud water path and water content are fixed (and thereby cloud physical thickness), as is k.

[9] Combining the signs of equations (3) and (5) with the fact that $\partial R_\lambda/\partial\tau_\lambda > 0$, means the dominant first term on the right hand side (RHS) of equation (1) is positive. This captures the essence of the first indirect effect argument. But the second and third terms in equation (1) can also contribute nontrivially to the albedo increase. Mie calculations show that in the shortwave part of the spectrum $d\overline{\omega}_\lambda/dr_e < 0$ and $dg_\lambda/dr_e > 0$ for typical cloud droplet size ranges. Given that $\partial R_\lambda/\partial\overline{\omega}_\lambda > 0$ and $\partial R_\lambda/\partial g_\lambda < 0$, all terms on the RHS of equation (1) are therefore positive, expressing the collective contribution of extinction, absorption, and scattering mechanisms to the albedo increase under constant water path conditions. For broadband calculations, the combined increase in susceptibility due to the 2nd and 3rd terms will be shown to be on the order of 10–30% through much of the expected liquid cloud τ, r_e space.

[10] While all terms in equation (1) are determined numerically with a broadband radiative transfer code for this study, analytic approximations are useful in understanding the functional dependencies. From equations (3) and (5), the dominant first term can be expressed as

$$\begin{aligned} S_\lambda(1) &= \frac{\partial R_\lambda}{\partial\tau_\lambda}\frac{d\tau_\lambda}{dr_e}\frac{dr_e}{dN} = \frac{\tau_\lambda}{3N}\frac{\partial R_\lambda}{\partial\tau_\lambda} = \frac{4\pi\rho_l}{9w}\tau_\lambda\frac{\partial R_\lambda}{\partial\tau_\lambda}kr_e^3 \\ S_\lambda^{rel}(1) &= \frac{\partial R_\lambda}{\partial\tau_\lambda}\frac{d\tau_\lambda}{dr_e}\frac{dr_e}{dN}N = \frac{\tau_\lambda}{3}\frac{\partial R_\lambda}{\partial\tau_\lambda} \end{aligned} \tag{6}$$

[see *Platnick and Twomey*, 1994]. Absolute susceptibility is found to have a cubic dependence on droplet size whereas relative susceptibility is not explicitly dependent on size when the optical thickness is specified. The second term in equation (1) has an approximate analytic form as well that can be derived from the *Hu and Stamnes* [1993] water cloud Mie scattering parameterizations used for broadband radiative flux calculations in this study (see section 3). Hu and Stamnes provide a parameterization for single-scattering coalbedo of the form $1-\overline{\omega}_\lambda\ (r_e) \approx c_{2,\lambda} + a_{2,\lambda} r_e^{b_{2,\lambda}}$ for three droplet size ranges, giving for susceptibility

$$\begin{aligned} S_\lambda(2) &\approx \frac{\partial R_\lambda}{\partial\overline{\omega}_\lambda}\frac{b_{2,\lambda}\left(1-\overline{\omega}_\lambda - c_{2,\lambda}\right)}{3N} \\ S_\lambda^{rel}(2) &\approx \frac{\partial R_\lambda}{\partial\overline{\omega}_\lambda}\frac{b_{2,\lambda}\left(1-\overline{\omega}_\lambda - c_{2,\lambda}\right)}{3} \end{aligned}. \tag{7}$$

For typical droplet size radii in the near-infrared to shortwave infrared where both solar radiation and droplet absorption ($1-\overline{\omega}_\lambda$) are significant, b_λ~0.8–1.0 and $c_\lambda \ll 1-\overline{\omega}_\lambda$. The magnitude of the ratio of the 2nd to 1st term in a spectral interval for both absolute and relative susceptibility is therefore approximated as being

$$\frac{S_\lambda(2)}{S_\lambda(1)} \approx \frac{(1-\overline{\omega}_\lambda)}{\tau_\lambda}\frac{\dfrac{\partial R_\lambda}{\partial\overline{\omega}_\lambda}}{\dfrac{\partial R_\lambda}{\partial\tau_\lambda}}. \tag{8}$$

Neglecting the partial derivatives, the second term becomes more significant as optical thickness decreases and absorption (r_e) increases. The derivatives cause the ratio to increase as the cloud becomes optically thick ($\partial R_\lambda/\partial\tau_\lambda \to 0$) and as absorption decreases ($\partial R_\lambda/\partial\overline{\omega}_\lambda$ increases with $\overline{\omega}_\lambda$). A similar parameterization from Hu and Stamnes for asymmetry parameter ($g_\lambda(r_e) = c_{3,\lambda} + a_{3,\lambda} r_e^{b_{3,\lambda}}$) contributes to the third term of susceptibility as

$$\begin{aligned} S_\lambda(3) &\approx \frac{\partial R_\lambda}{\partial g_\lambda}\frac{b_{3,\lambda}\left(g_\lambda - c_{3,\lambda}\right)}{3N} \\ S_\lambda^{rel}(3) &\approx \frac{\partial R_\lambda}{\partial g_\lambda}\frac{b_{3,\lambda}\left(g_\lambda - c_{3,\lambda}\right)}{3} \end{aligned}, \tag{9}$$

giving the magnitude of the ratios of equation (9) to equation (6) as

$$\frac{S_\lambda(3)}{S_\lambda(1)} \approx \frac{b_{3,\lambda}\left(g_\lambda - c_{3,\lambda}\right)}{\tau_\lambda}\frac{\dfrac{\partial R_\lambda}{\partial g_\lambda}}{\dfrac{\partial R_\lambda}{\partial\tau_\lambda}}. \tag{10}$$

The 3rd term once again becomes more significant at small and large optical thicknesses. While the coefficients $b_{3,\lambda}$ and $c_{3,\lambda}$ in the numerator reflect the fact that dg_λ/dr_e can vary substantially as a function of wavelength and droplet size, the derivative is larger at smaller radii. Example broadband calculations for albedo susceptibility and these ratios will be shown in section 4.

2.2. Numerical Evaluation

[11] The numerical evaluation of susceptibility starts by determining the Δr_e corresponding to a finite perturbation ΔN or $\Delta N/N$. From equation (4), the effect of relative and absolute droplet number perturbations on effective radius for a constant water content process are derived as follows:

$$\begin{aligned} \frac{\Delta r_e}{r_e} &= \left(\frac{1}{1+\dfrac{\Delta N}{N}}\right)^{\frac{1}{3}} - 1, \text{ specify}\frac{\Delta N}{N} \\ &= \left(\frac{1}{1+\dfrac{4\pi\rho_l}{3}\dfrac{\Delta N}{w}kr_e^3}\right)^{\frac{1}{3}} - 1, \text{ specify}\Delta N, w \\ &= \left(\frac{1}{1+2\pi\rho_l\dfrac{\Delta N}{\tau}Hkr_e^2}\right)^{\frac{1}{3}} - 1, \text{ specify}\Delta N, H. \end{aligned} \tag{11}$$

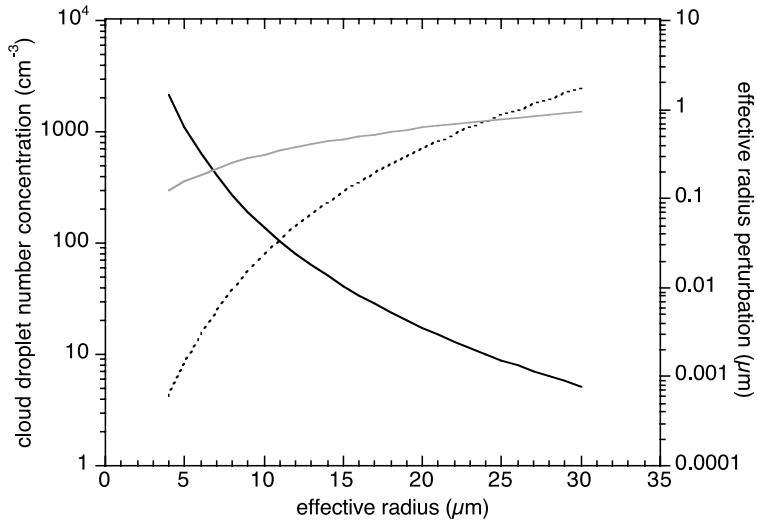

Figure 1. Cloud droplet number concentration (N) for a liquid marine cloud ($k = 0.83$) with liquid water content $w = 0.3$ gm^{-3}, as a function of effective radius r_e (solid line, left axis). Also shown is the negative of the effective radius perturbation Δr_e (dashed curve) for $\Delta N = 1$ cm^{-3} and $\Delta N/N = 10\%$ (gray curve).

For small $\Delta N/N$, $\Delta r_e/r_e \approx -\Delta N/3N$, which is equivalent to the differential form of equation (5). Note that the assumed linear relationship $r_v^3 \propto r_e^3$ is implicit in the perturbation corresponding to specifying $\Delta N/N$, while a ΔN perturbation also requires knowledge of the constant of proportionality k.

[12] Resulting changes in τ_λ, $\overline{\omega}_\lambda$, g_λ from the droplet size perturbations of equation (11) can be used to directly evaluate susceptibility (equation (1)) from:

$$\Delta R_\lambda = R_\lambda(\tau_\lambda + \Delta\tau_\lambda, \overline{\omega}_\lambda + \Delta\overline{\omega}_\lambda, g_\lambda + \Delta g_\lambda) - R_\lambda(\tau_\lambda, \overline{\omega}_\lambda, g_\lambda). \tag{12}$$

From equations (2) and (11), the effect of a droplet size perturbation on optical thickness is

$$\tau_\lambda + \Delta\tau_\lambda = \tau_\lambda\left(\frac{1}{1 + \frac{\Delta r_e}{r_e}}\right), \tag{13}$$

which reduces to the differential analog of equation (3). Note that relative changes in spectral optical thickness are not wavelength-dependent. For completeness, we note that parameterizations from *Hu and Stamnes* [1993] and *Chou et al.* [1998] are used to determine the perturbations to the other radiative parameters:

$$\begin{aligned} \overline{\omega}_\lambda + \Delta\overline{\omega}_\lambda &= \overline{\omega}_\lambda(r_e + \Delta r_e) \\ g_\lambda + \Delta g_\lambda &= g_\lambda(r_e + \Delta r_e) \end{aligned}. \tag{14}$$

In summary, once the effective radius change due to a specified droplet number perturbation is found from equation (11), equations (13) and (14) can be evaluated for use in equation (12). For our susceptibility calculations with the GSFC solar radiative transfer code (see next section), changes in spectral optical thickness, single-scattering albedo, and asymmetry parameter are handled internally by the broadband model by passing in the fixed cloud water path and the effective radius perturbation.

[13] Equations (12)–(14) make it clear that at a minimum, both optical thickness and effective radius are required to calculate cloud susceptibility. The practical advantage to specifying a relative droplet number perturbation is that no other cloud parameter is needed. In particular, note that the dominant term (equation (6)) has no explicit dependence on r_e once the optical thickness is specified (but the dependence is implicit in $\partial R_\lambda/\partial\tau_\lambda$ which varies with r_e). However, if a ΔN perturbation is specified, then either N needs to be known (equivalent to specifying the relative perturbation) or else a cloud microphysical (w) or macrophysical (H) quantity is required, in addition to a value for the parameter k. Here (as in the work by *Platnick and Twomey* [1994]) $\Delta N = 1$ cm^{-3} is used to obtain numerical estimates of absolute susceptibility and $w = 0.3$ gm^{-3} is chosen as the normalization For other values of w (in gm^{-3}), absolute susceptibility can be approximated by using the scaling factor $0.3/w$, though this is exact only for the first term in equation (1a). In a similar manner, while the parameter k is set to 0.83 for all subsequent calculations, absolute susceptibility can be scaled to other k values. Figure 1 shows N as a function of r_e for $w = 0.3$ gm^{-3} as derived from equation (4). The resulting values of N for r_e ranging between 4 and 20 μm span about two orders of magnitude. N for other water content values can be derived by scaling the curve by $w/0.3$. The corresponding negative perturbations in effective radius, Δr_e, for $\Delta N = 1$ cm^{-3} and $\Delta N/N = 10\%$ are also shown in Figure 1 (dashed and gray curves, respectively) where the sign of Δr_e has been reversed to accommodate the logarithmic scale. For absolute susceptibility ($\Delta N = 1$ cm^{-3}), Δr_e perturbations for clouds with small r_e are 2–3 orders of magnitude smaller than clouds with large r_e, while the Δr_e range is much narrower for the $\Delta N/N = 10\%$ perturbations. It should be noted that the $w = 0.3$ gm^{-3} assumption applied for absolute

susceptibility calculations in this paper does not always yield commonly occurring values of N.

2.3. Assumptions and Error Budget

[14] If the assumption of constant k, w, and H during the droplet perturbation process are relaxed, the first term in absolute susceptibility becomes $S(1)[1 + d\ln k/d\ln N + 2d\ln w/d\ln N + 3d\ln H/d\ln N]$ [*Ackerman et al.*, 2000]. The first additional term shows that when a spectral broadening (smaller k) is associated with increasing N (condensation-dominated process, e.g., polluted conditions), $S(1)$ decreases; when broadening is associated with decreasing N (coalescence-domination process, e.g., clean conditions), $S(1)$ increases [*Feingold and Seibert*, 2008]. The second and third terms show that $S(1)$ increases if water content or physical thickness increases with N. While this provides perspective regarding the implications of fixed water amount and k, it is not feasible to set values for these additional sensitivities for global satellite studies. Cloud fraction sensitivities to N would present an additional issue (impact depends on surface albedo).

[15] Expressions derived for constant N and adiabatic cloud processes can also be investigated for absolute susceptibility studies. Adiabatic processes give rise to water content linear in height for typical water cloud thicknesses and temperatures (e.g., $w(h) = C_w h$ using the notation of *Brenguier et al.* [2000], with C_w as the moist adiabatic coefficient), yielding a maximum effective radius at cloud top. If one assumes that the effective radius retrieved from solar reflectance observations, r_e^*, corresponds exactly to the adiabatic effective radius at cloud top, H, then the ratio of $N/w(H)$ is known at cloud top (equation (4)); if C_w is assumed known, then N/H is also known. Finally, the retrieved cloud optical thickness is an integration over a vertically increasing effective radius, and so can be used to solve for H which thereby gives N. The constant droplet concentration can then be expressed as

$$N = \frac{1}{2\pi k}\left(\frac{5}{\rho_l \overline{Q}_\lambda}\right)^{1/2} C_w^{1/2}\tau_\lambda^{1/2} r_e(H)^{-5/2} \qquad (15)$$

[see also *Quaas et al.*, 2006]. Note that k is assumed independent of height in this analysis. With the solar retrievals providing τ_λ and $r_e(H) \approx r_e{*}$ for this derived N, a ΔN perturbation can be transformed to a relative perturbation and absolute susceptibility no longer requires microphysical assumptions. But instead of having to assume w, for example, one has to assume a value for C_w dependent on the unknown cloud base temperature. Even if the cloud is adiabatic, retrieved radii are not exactly at cloud top but can be ~5–15% less than at cloud top depending on geometry and effective radius profile [*Platnick*, 2000]. The assumption of a constant N with height is common to both equations (4) and (15).

[16] Satellite studies using combined microwave and solar retrievals suggests that marine stratocumulus clouds off the subtropical western continental coasts are often adiabatic in character [*Bennartz*, 2007]. The overall uncertainty in retrieving N from equation (15) for such clouds can be estimated assuming the uncertainties for individual error sources are uncorrelated. Using a relative uncertainty of 10% for both k and C_w for these adiabatic-like clouds [*Bennartz*, 2007], and 10% and 20% for τ_λ and $r_e(H)$, respectively (for typical subtropical solar zenith angles, optical thicknesses, MODIS instrument calibration, vertically homogeneous r_e assumption, etc.), the overall uncertainty in the retrieval of N would be about 50% for these cloud types (see *Bennartz* [2007] for error propagation formula). In contrast, the uncertainty in N from equation (4) is ~75% (same individual uncertainties for k and r_e, and using 50% for $w = 0.3$ gm^{-3}).

[17] Equations (4) and (15) for N can be substituted into equation (6) to assess the overall uncertainty in the first term of absolute susceptibility. Ignoring the uncertainty in the partial derivative, both the adiabatic and vertically homogeneous absolute susceptibility uncertainties are dominated by the uncertainty in N (i.e., negligibly greater than the 50% and 75% uncertainty in N alone for the example in the preceding paragraph). Note that relative susceptibility uncertainties are dominated by the uncertainty in τ_λ which is expected to be much smaller. While there is some potential reduction of uncertainty in deriving absolute susceptibility for adiabatic cloud regimes via equation (15), it is not obviously significant in light of the requirement of adiabatic clouds in addition to constant N. Moreover, the radiative transfer code used for the analysis would have to divide the cloud into sublayers in order to resolve the profile, complicating the calculations. For these reasons we use equation (4) for all calculations of absolute susceptibility that follow.

[18] These uncertainty estimates are for a single observation (pixel); susceptibility statistics derived from aggregations (as in Part 2) will be reduced by the inverse of the square root of the number of observations if pixel-to-pixel errors are uncorrelated. Though this is perhaps optimistic, a significant reduction in the aggregated uncertainty is expected.

2.4. Transmittance and Absorptance Susceptibilities

[19] The cloud transmitted flux, T_λ, and its absolute and relative susceptibilities ($S_{T_\lambda} = dT_\lambda/dN$ and $S_{T_\lambda}^{rel} = dT_\lambda/d\ln N$) are of interest for surface radiation studies. Since the transmitted flux decreases with cloud optical thickness, the counterpart to the first term on the RHS of equation (1a) is negative. The second term is positive because $\partial T_\lambda/\partial\overline{\omega}_\lambda > 0$, while the third term is negative because $\partial T_\lambda/\partial g_\lambda > 0$. As before, the first term is typically dominant making the overall transmittance susceptibility negative; that is, a positive droplet number perturbation reduces the cloud transmittance.

[20] We now consider absorption perturbations for the entire atmospheric column (clear as well as cloudy layers) including interactions with the surface, in which case reflectance and transmittance susceptibilities correspond to the top-of-atmosphere and surface, respectively. The fractional spectral flux absorbed at the surface ($A_{\mathrm{sfc},\lambda}$) is given by $(1 - r_\lambda)T_\lambda$, r_λ being the spectral albedo of the surface and T_λ understood to be the net transmittance. The absolute surface absorptance susceptibility to a cloud microphysical perturbation is therefore

$$S_{Asfc_\lambda} = \frac{dA_{sfc_\lambda}}{dN} = (1 - r_\lambda)\frac{dT_\lambda}{dN} = (1 - r_\lambda)S_{T_\lambda}, \qquad (16)$$

with a similar form for relative susceptibility. The atmospheric absorptance is $A_\lambda = 1 - R_\lambda - A_{\mathrm{sfc},\lambda} = 1 - R_\lambda - (1 - r_\lambda)T_\lambda$, giving absolute atmospheric absorptance susceptibility as

$$S_{A_\lambda} = \frac{dA_\lambda}{dN} = -\frac{dR_\lambda}{dN} - (1 - r_\lambda)\frac{dT_\lambda}{dN} = -S_\lambda - (1 - r_\lambda)S_{T_\lambda}, \quad (17)$$

where the nonsubscripted susceptibility is understood to be for albedo. For no atmospheric absorption (cloud or gas) and a black surface, the values of the albedo and transmittance susceptibility are, of course, of equal and opposite sign. Example broadband calculations of absorptance susceptibility will be discussed in sections 4 and 5.

[21] Unless specifically noted, susceptibility results in subsequent sections represent flux perturbations for the entire atmospheric column, i.e., surface plus cloud plus clear sky scattering and absorption, with reflectance susceptibilities referenced to the top-of-atmosphere. Absolute susceptibilities are given in mm^3 and relative susceptibilities have been multiplied by 1000.

3. Susceptibility Calculations With a Broadband Radiative Transfer Model

[22] Susceptibility calculations were performed with the broadband solar radiation code used in GSFC Large Scale Models [*Chou et al.*, 1998; *Chou and Suarez*, 2002]. The model calculates flux profiles over the entire solar spectrum (0.2–5 μm) or over UV-VIS (0.2–0.7 μm) and NIR (0.7–5 μm) bands separately. The UV-VIS is resolved into a single band, while the NIR is resolved into three separate bands for which cloud properties are assumed to be spectrally flat. The model can account for molecular, aerosol, and cloud absorption and scattering, and surface reflection with and without a vegetation canopy. Multiple scattering is handled by a delta-Eddington approximation to the radiative transfer equation. Since our calculations pertain to overcast conditions only, the overlap assumptions of the model are not used. The surface and atmosphere can be switched off, allowing for calculations that isolate the cloud-only albedo, transmittance and absorptance.

[23] In the original model, the band-averaged droplet single-scattering properties are parameterized as function of r_e within the range of 4 to 20 μm using polynomial fits. Extending the polynomial fits outside the range for which they were derived, leads to incorrect (negative) sign for the derivatives $d\overline{\omega}_\lambda/dr_e$ and dg_λ/dr_e in most spectral bands. This portion of the model therefore needed to be modified. In the new version, estimation of single-scattering properties is now possible over the size range 3–30 μm. This was achieved in the following manner. The tables of SBDART [*Ricchiazzi et al.*, 1998] containing an enhanced spectral resolution version of the regression parameters of the *Hu and Stamnes* [1993] parameterization were used to calculate the spectrally variable extinction coefficient, g_λ, and $\overline{\omega}_\lambda$ for effective radii r_e = 3, 4, 5, ... 30 μm. The procedure of *Chou et al.* [1998] was then used to average across the four spectral bands of the radiative transfer model for each effective radius, thus forming look-up tables of single-scattering properties as a function of r_e. When running the code for arbitrary (noninteger) values of effective radii, linear interpolation is used to obtain nontabulated values of single-scattering properties. The exception to this parameterization approach is in the midwave infrared spectral region (band 4) where dg_λ/dr_e calculated from the Hu and Stamnes fit has a substantial change in curvature near r_e = 12 μm, causing spurious derivative calculations. Fortunately, the Chou et al. fit for this band is well behaved across the entire effective radius range and is therefore used instead. Regardless, there is no noticeable difference in susceptibility statistics between the two fits for MODIS data granule (pixel-level) and gridded (see Part 2) susceptibilities. Improved single-scattering property parameterizations suitable for sensitivity (derivative) calculations are clearly needed, but are beyond the scope of this study.

[24] The flux calculations of this study are performed as follows: The optical thickness value for a given τ, r_e pair is considered to correspond to the model's UV-VIS band (band 1). From the extinction that corresponds to the given value of r_e for that band, the liquid water path W is calculated. The W, r_e pair is then used as input to the radiative transfer algorithm for the calculation of optical thickness in the other bands, and of the unperturbed radiative flux, in the usual way. Susceptibility and relative susceptibility calculations are carried out with the GSFC code for two subcases: one where all terms on the RHS of equation (1) are accounted for ("all-term") and one where only the dominant first term ("one-term") is retained. For "all-term" susceptibility and relative susceptibility calculations, the perturbed value of effective radius ($r_e + \Delta r_e$) as described in section 2 is used to obtain a new (perturbed) radiative flux. On the other hand, for one-term susceptibility or relative susceptibility, $r_e + \Delta r_e$ is used only to calculate a new value of extinction coefficient, while the unperturbed (original) r_e is used for the calculation of single-scattering albedo and asymmetry parameter; thus, equation (6) is approximated internally by the radiative transfer model. Changes in broadband albedo are calculated from the model as described in section 2.2, i.e.,

$$\Delta R = \frac{\sum_i f_i F_i^{\uparrow}(\tau_i + \Delta\tau_i, \overline{\omega}_i + \Delta\overline{\omega}_i, g_i + \Delta g_i)}{\mu_0 F_0^{\downarrow}} - \frac{\sum_i f_i F_i^{\uparrow}(\tau_i, \overline{\omega}_i, g_i)}{\mu_0 F_0^{\downarrow}}, \quad (18)$$

where $\Delta\tau_i$, Δg_i and $\Delta\overline{\omega}_i$ perturbations are due to $\Delta r_e < 0$ perturbations arising from changes $\Delta N > 0$ or $\Delta N/N > 0$ (see equation (11)). The other symbols in the above equation are: i is the model's spectral band index (i = 1,...4), μ_0 is the cosine of the solar zenith angle (SZA), $F_0^{\downarrow}$ is incident solar irradiance at the top of the atmosphere (TOA), $F_i^{\uparrow}$ is the spectral flux reflected back to space at the TOA, and f_i is the fractional relative contribution to $F_0^{\downarrow}$ in band i. A similar expression applies for ΔT.

[25] With this broadband radiative transfer code, calculations can be made for albedo, transmittance, surface and atmospheric absorptance, and their susceptibilities for the UV-VIS and NIR portions of the solar spectrum under cloudy (liquid phase) conditions with and without surface and atmospheric effects for a specific SZA. "Spherical" albedos, transmittances, absorptances and corresponding

susceptibilities can be defined by integrating over the full range of SZA angles. Since susceptibility is derived numerically, the behavior of radiative perturbations for an arbitrary ΔN can also be examined. This is especially relevant when changes in droplet concentration come from a cloud microphysical model where specific emission scenarios determine the number of CCN. However, such a case is not examined here.

4. Theoretical Results

4.1. Albedo, Transmittance, and Absorptance Susceptibilities

[26] Figure 2 (top) shows values of broadband albedo, and absolute and relative albedo susceptibility for a wide range of r_e (4–30 μm) and τ (0.5–100) corresponding to the MODIS retrieval space. The r_e and τ increments are 1 μm and 0.5, respectively. The SZA is set to 60°. The surface is black and atmospheric effects are ignored.

[27] The dependence of absolute albedo susceptibility on effective radius reflects the dominant first susceptibility term of equation (1) as expressed by equation (6), namely the r_e^3 dependence; for conservative scattering, the transmittance susceptibility must be equal and opposite to that for albedo (section 2.4) and therefore also possess a r_e^3 dependence. For a particular value of r_e, the maximum albedo susceptibility occurs where the product $\tau\partial R/\partial\tau$ is maximum. *Platnick and Twomey* [1994] have shown that this occurs for conservative scattering at values of cloud albedo ~0.5 (see Figure 9, bottom; also demonstrated in Part 2). This is roughly consistent with Figure 2 (top right and top middle), and for SZA = 60° occurs at values of τ~8. For relative albedo susceptibility there is a much smaller droplet size dependence for a fixed optical thickness, with values increasing as r_e decreases (due to $\partial R/\partial\tau$ increasing as size decreases for a constant τ as a result of the influence of $\overline{\omega}$ and g on the reflectance curvature).

[28] Figure 2 (bottom) shows plots for flux transmittance, and absolute and relative cloud absorptance susceptibility. Though albedo and transmittance contours have significantly different patterns in the τ, r_e phase space, the corresponding transmittance susceptibilities (not shown) are remarkably similar. Transmittance is rather insensitive to r_e as a result of the competing effects of g and $\overline{\omega}$: as r_e increases, the resulting increase in asymmetry parameter moves the transmittance toward higher values while the decrease in single-scattering albedo moves the transmittance toward lower values (in the case of albedo, both single-scattering parameters would move the albedo toward lower values). Yet, the absolute transmittance susceptibility is as strongly dependent on r_e as the absolute albedo susceptibility. With small differences in the magnitudes of broadband albedo and transmittance susceptibilities, cloud absorptance susceptibilities are an order of magnitude smaller and have different functional shapes than their albedo counterparts. Note that the absorptance susceptibilities are negative throughout much of the space, but become positive for small optical thicknesses and larger radii (i.e., a droplet concentration perturbation results in the cloud absorbing more radiation as the broadband transmittance perturbation decreases faster than the albedo perturbation increases).

4.2. Contributions From Different Scattering Parameter Terms

[29] Example broadband calculations for the ratios of various terms in equation (1) that were discussed in section 2.1 are shown in Figure 3. As in section 4.1, calculations are for an isolated cloud (i.e., black surface and no atmosphere). Figure 3 (top left) shows that $S(1)$ is within about 10–30% of the all-term calculation for clouds with optical thickness less than about 30. Single-scattering albedo and asymmetry parameter perturbations can potentially have much larger relative contributions, adding an extra ~80% to $S(1)$ for the larger optical thicknesses. Statistics from example MODIS retrievals in the next section will show that differences of about 15% are more representative of those scenes.

[30] Figure 3 (top middle and top right) shows broadband calculations corresponding to equations (8) and (10); the inverse of the denominator in both these equations is shown in Figure 3 (bottom right) indicating an abrupt increase at the smallest optical thicknesses (τ~1) and a more gentle increase at large optical thickness as expected. The $S(2)/S(1)$ and $S(3)/S(1)$ ratios are functionally consistent with the discussion in section 2.1, with the exception that the impact of the smallest optical thicknesses is not noticeable with the chosen discrete color bars and is indicative that some damping of the τ^{-1} term is occurring because of the partial derivative in the numerator.

[31] It must be stressed that the methodology used in this study to estimate susceptibility does not gain any logistical or computational advantages by neglecting $\Delta\overline{\omega}$ and Δg perturbations. We mainly examine this issue to understand how our approach can contribute to the interpretation of previously published results and to gauge the importance of parameterizations for $\overline{\omega}(r_e)$ and $g(r_e)$. In that spirit, Figure 3 also shows a calculation for the all-term to one-term UV-VIS (<0.7 μm) susceptibility ratio since the latter most closely approximates the susceptibility as calculated by previous studies [e.g., *Platnick and Twomey*, 1994]. Except for the smaller radii, this portion of the spectrum contributes more than about 85% to the overall cloud albedo susceptibility through the expected τ, r_e space. The ratios are closer to unity than for $S/S(1)$ because $(\partial R/\partial\tau)_{UV\text{-}VIS} > \partial R/\partial\tau$. The contribution of $\Delta\overline{\omega}$ and Δg perturbations on susceptibility is revisited in section 5 with MODIS-derived results that also include atmospheric effects.

4.3. Dependence on Solar Zenith Angle

[32] Since cloud albedo is a function of SZA, susceptibility, being proportional to an albedo difference, should also have some dependence on SZA. Figure 4 provides a glimpse into this dependence (absolute and relative susceptibilities shown in the top and bottom rows, respectively). To isolate the susceptibility of the cloud itself, atmospheric and surface effects are again ignored. The first column from the left corresponds to SZA = 60°, the second column to SZA = 0°, and the third column comes from spherical albedo calculations (i.e., cosine-weighted integration of albedo from μ_0 = 0 to 1). For both absolute and relative susceptibility, the area covered by values close to the maximum is smallest for SZA = 60°. Outside the region of maximum susceptibility, it is harder to assess any differences from these figures. To examine the susceptibility

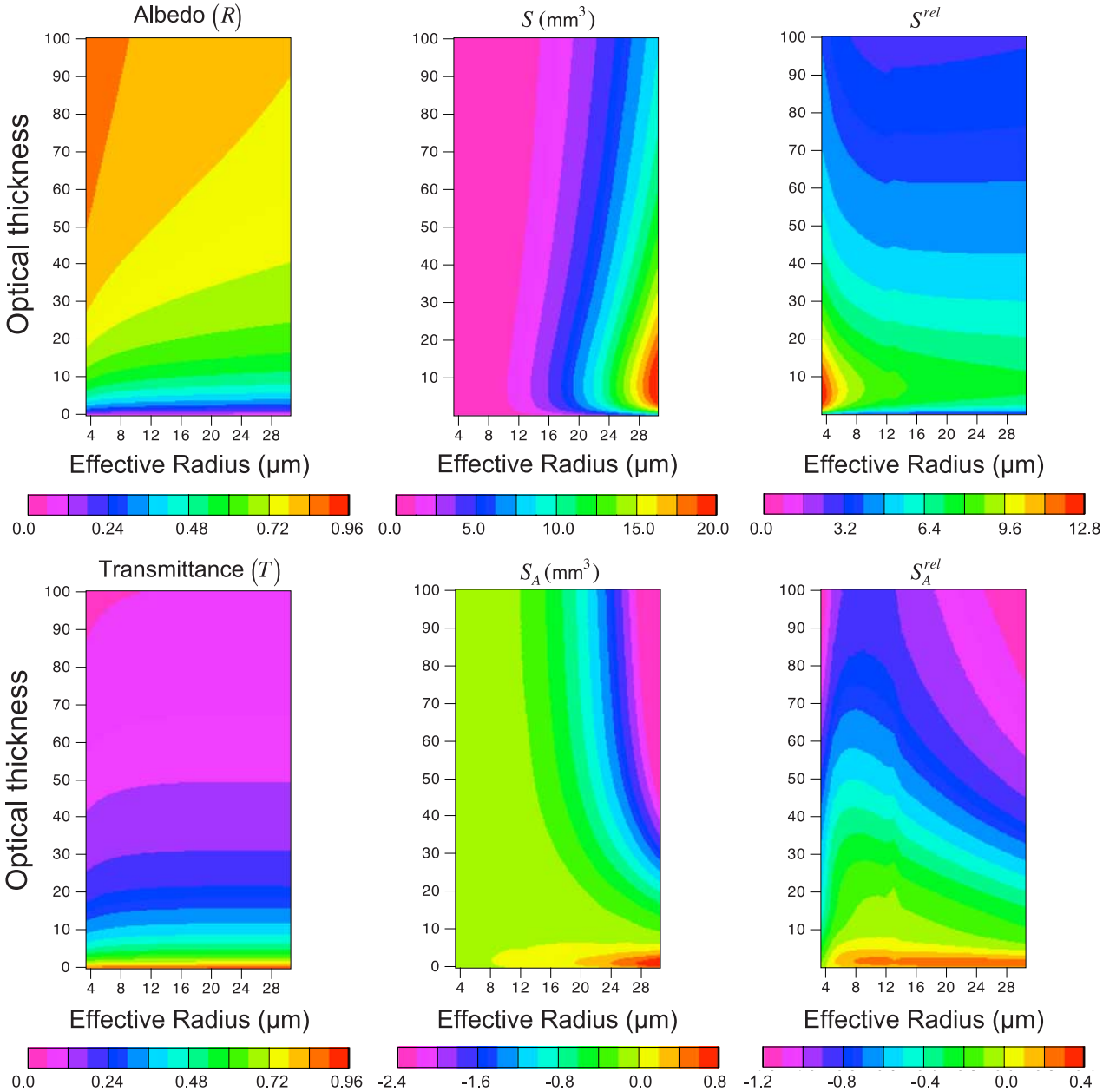

Figure 2. (top) Theoretical calculations of broadband albedo, absolute albedo susceptibility, and relative albedo susceptibility as a function of cloud optical thickness and effective radius. (bottom) Counterpart calculations for transmittance, absolute absorptance susceptibility, and relative absorptance susceptibility. Absolute susceptibility calculations are for $\Delta N = 1$ cm^{-3}, $w = 0.3$ gm^{-3}, and relative susceptibility calculations are for $\Delta N/N = 10\%$, with contributions from all derivative terms. The solar zenith angle is 60°. Calculations do not include atmospheric gases and are for a black surface. Relative susceptibilities have been multiplied by 1000.

dependence across the full range of SZA in more detail, Figure 5 plots susceptibilities as a function of the cosine of the SZA for $\tau = 10$ and $r_e = 10$ μm. The spherical susceptibility for this τ, r_e pair is included as well. The ratio of absolute to relative susceptibility remains constant with SZA, thus both susceptibilities are represented by a single (solid) curve. The dependence of susceptibility on SZA is quite strong (maximum value is about double the minimum value considered) with the expected increase as the solar elevation increases and the tendency for albedo saturation effects diminishes. In an application where susceptibility needs to be expressed in radiative flux terms, the μ_0 dependence is relevant (dashed curve) so that large SZAs are even less important energetically to droplet concentration perturbations. In the presence of an absorbing atmosphere and a reflecting surface these results would be more dramatic (see section 4.4). Hence, identical clouds within an identical environment would have much smaller TOA susceptibilities at high latitudes than at low latitudes.

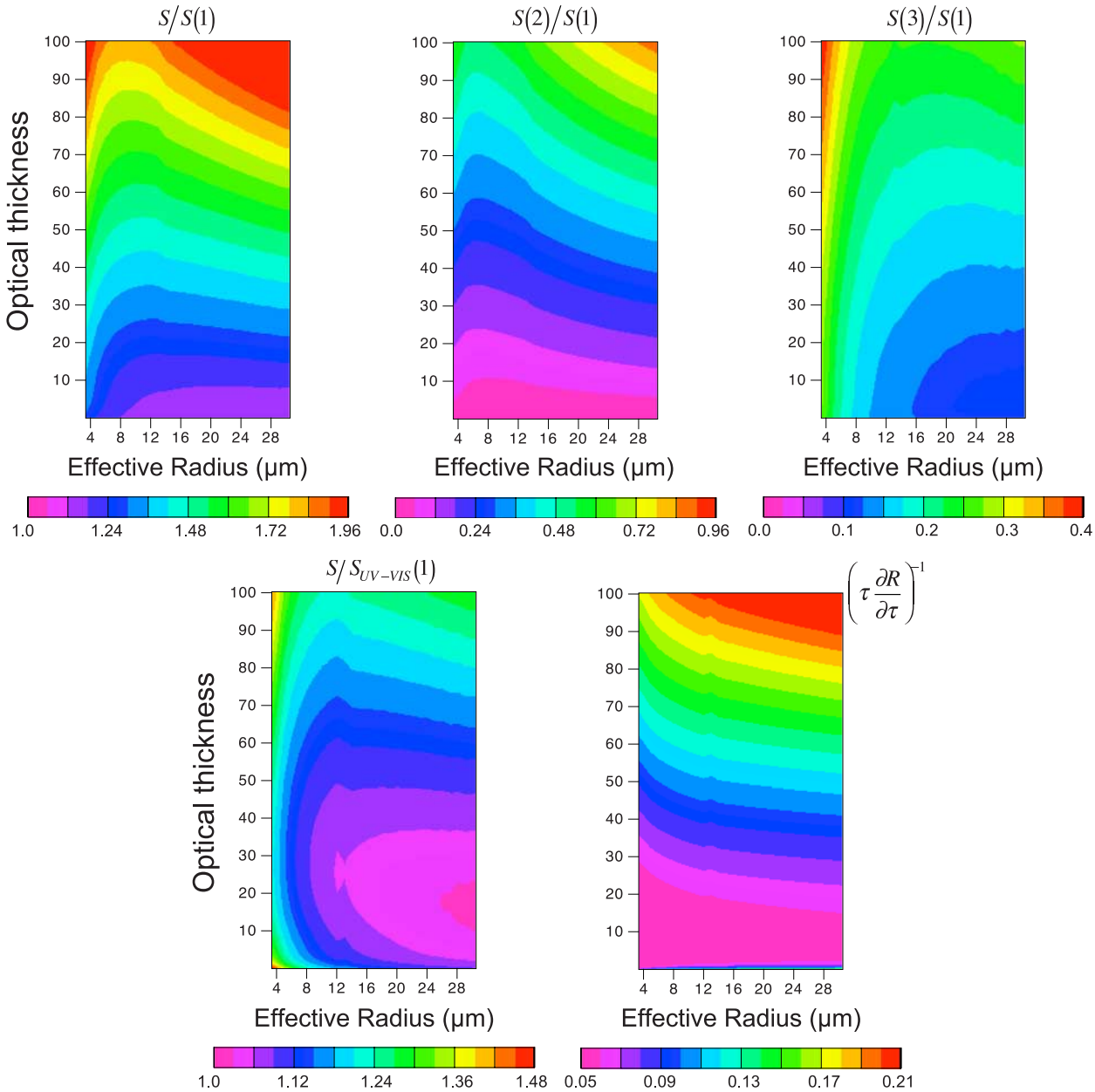

Figure 3. Ratio of various broadband albedo susceptibility terms as a function of cloud optical thickness and effective radius (e.g., S is all terms in equation (1), $S(1)$ is the first term, $S_{UV\text{-}VIS}(1)$ is the first term for only the UV through visible portion of the spectrum, etc.). The ratios are the same for either absolute or relative susceptibility. Calculations are for no atmosphere and a black surface. The solar zenith angle is 60°.

4.4. Other Dependencies

[33] When a cloud is embedded in an absorbing and scattering atmosphere and/or when a cloud is present over a reflecting surface, albedo susceptibility decreases. This can be understood by considering the reduced role of the cloud in determining the TOA albedo. The decrease in susceptibilities (relative or absolute) from cloud-only values becomes more significant as the surface becomes more reflective, the atmosphere becomes more absorbing or reflective, and the cloud becomes optically thinner. Figure 6 (left) shows an example for a cloud embedded in a standard midlatitude summer atmosphere and overlying a surface with a spectrally flat albedo of 0.2. The SZA is again 60°. Reductions of 30–50%, driven mainly by the surface albedo, can be easily reached. These results have obvious importance in assessing the real world TOA radiative susceptibility: for similar cloud properties and microphysical modifications, clouds over bright surfaces and/or in moist environments are not as radiatively important as those over dark surfaces and/or in dry environments.

[34] Two more issues need to be addressed: scaling for particular values of liquid water content (w) and linearity to

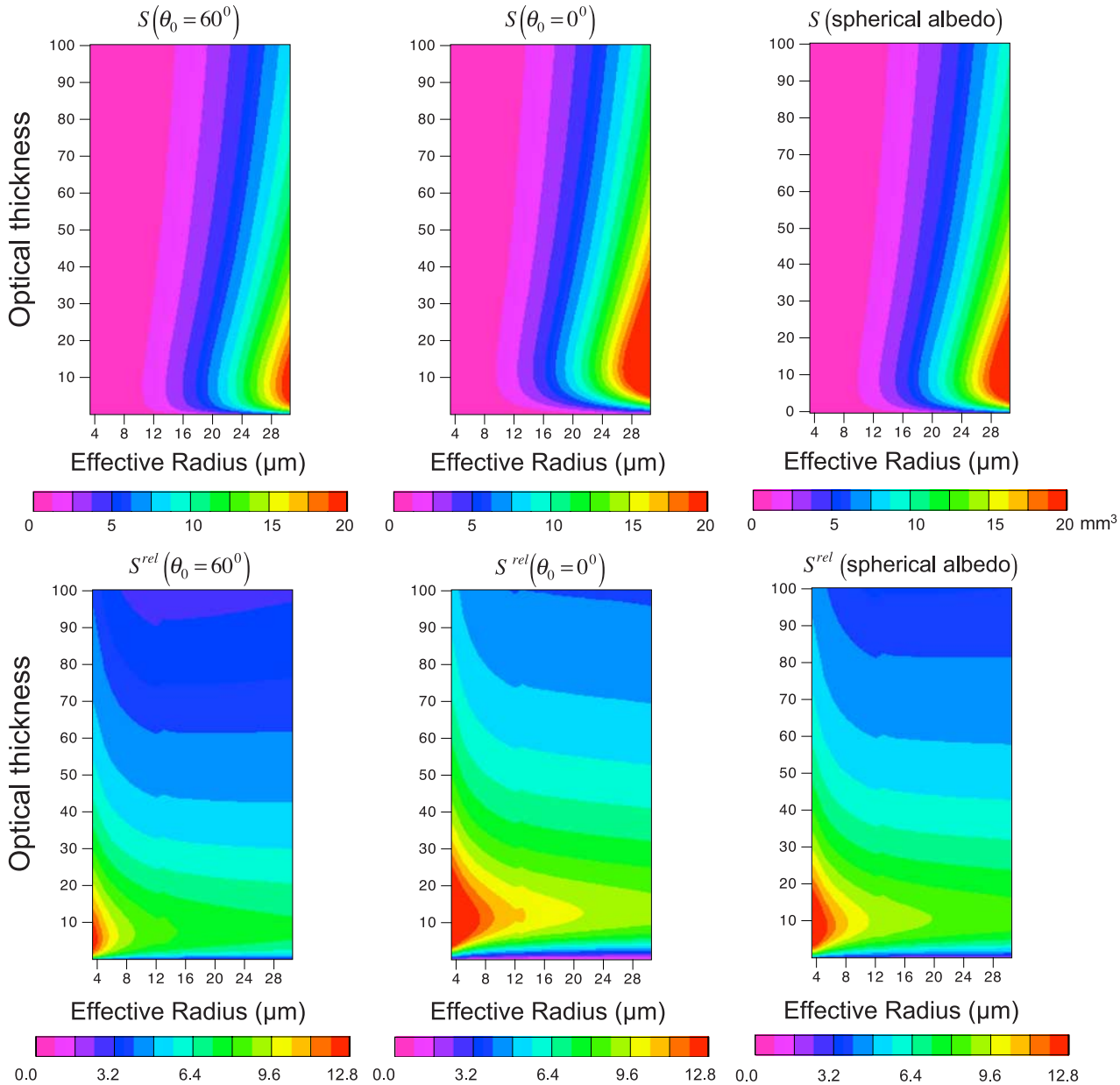

Figure 4. Dependence of absolute and relative albedo susceptibility on solar geometry. (top) Absolute (ΔN = 1 cm^{-3}, w = 0.3 gm^{-3}) susceptibility and (bottom) relative ($\Delta N/N$ = 10%) susceptibility. (left) Solar zenith angle SZA = 60°, (middle) SZA = 0°, and (right) susceptibility for spherical albedo. No atmosphere or surface albedo effects are present. Relative susceptibilities have been multiplied by 1000.

$\Delta N/N$ perturbations in the absolute and relative susceptibility calculations, respectively. For one-term susceptibility calculations, the scaling is found from equations (11)–(13) to be roughly inversely proportional to the fractional change in w. There is little change to the scaling when $\Delta\varpi$ and Δg perturbations are included according to the all-term calculations shown in Figure 6 (middle) (which does not include atmospheric and surface effects). Reducing w by a third increases absolute susceptibility by about 50% over the entire τ, r_e domain. As a test of linearity, doubling $\Delta N/N$ approximately doubles the albedo perturbation over the entire τ, r_e domain (Figure 6, right) even in the presence of $\Delta\varpi$ and Δg perturbations. These results emphasize again the dominance of the extinction perturbation term.

5. MODIS Data Granule Results

[35] Susceptibility fields were calculated from liquid water cloud retrievals in two Collection 5 MODIS Terra Level 2 Joint Atmosphere Product data granules (product name MODATML2). These granules were selected as representative of two widely different climatological cloud regimes and illustrate how susceptibility can be calculated from satellite passive measurements.

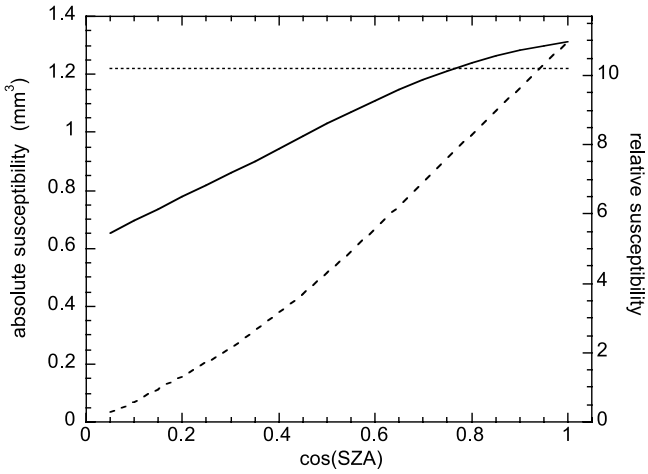

Figure 5. Absolute (ΔN = 1 cm^{-3}, w = 0.3 gm^{-3}, left axis) and relative ($\Delta N/N$ = 10%, right axis) albedo susceptibilities as a function of the cosine of solar zenith angle (SZA) for τ = 10 and r_e = 10 μm and no atmospheric or surface albedo effects present. The ratio of absolute to relative susceptibility remains constant with SZA; thus both are represented by a single (solid) line. The horizontal dotted line is the spherical albedo susceptibility. The dashed curve is the product of susceptibility and cos(SZA) which captures the effect of solar angle on energy-weighted calculations. Relative susceptibility has been multiplied by 1000.

[36] The MODIS Atmosphere Level 2 Joint Product contains key Scientific Data Sets (SDSs) selected from the operational Level 2 aerosol, water vapor, atmospheric profile, cloud properties, and cloud mask product files. Many SDSs contained within the Joint Atmosphere product are at reduced spatial resolution: the cloud products of interest here [*Platnick et al.*, 2003] are subsampled at 5 km resolution from the original 1 km resolution. Since the reduction in data volume comes from subsampling rather than averaging, our calculations aiming to demonstrate the links among cloud properties, solar geometry, surface albedo, and susceptibility are not affected. Summary information on these two granules is provided in Table 1. True color composite images and geographic location information are shown in Figure 7.

[37] Ancillary surface spectral albedo for the radiative transfer calculations comes from the identical data sources and methods used in the operational MODIS Terra cloud retrievals (product MOD06). The snow-free land surface albedo comes from the 5-year climatology of *Moody et al.* [2005], which uses an ecosystem-dependent temporal interpolation technique to fill missing or seasonally snow covered data in the operational MODIS Terra surface albedo product (MOD43B3). The data are provided in a 1 arc minute equal angle grid with the seasonal cycle resolved into 16-day periods. We use the diffuse ("white sky") albedo for the broad 0.3–0.7 μm and 0.7–5.0 μm spectral ranges, roughly corresponding to the UV-VIS and NIR bands of the *Chou et al.* [1998] model, for the specific 16-day period containing the data granule observation. The latitude and longitude data contained in the Level 2 joint product are used in an interpolation scheme to obtain the surface albedo for each sampled pixel. Ocean diffuse incident albedo values are set to 0.05 in both spectral ranges of the Moody et al. data set.

[38] Atmospheric profiles of temperature and water vapor used in the radiative transfer model are resolved into 16 layers extending from 1000 to 10 mbar and come from

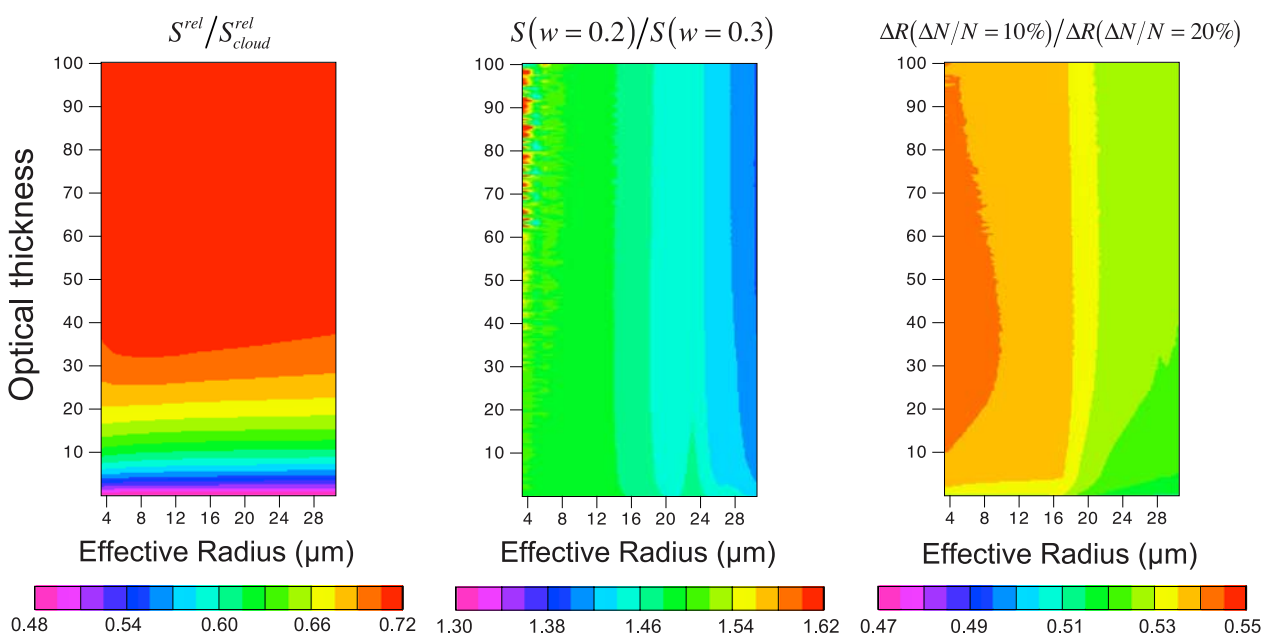

Figure 6. (left) Ratio of a relative susceptibility calculation ($\Delta N/N$ = 10%) that imbeds the cloud in a standard midlatitude atmosphere over a spectrally flat surface albedo of 0.2 to a cloud-only calculation (no atmosphere, black surface). (middle) Ratio of absolute susceptibility for w = 0.2 gm^{-3} to w = 0.3 gm^{-3} and ΔN = 1 cm^{-3} (cloud-only). (right) Ratio of albedo perturbations for $\Delta N/N$ = 10% to $\Delta N/N$ = 20% (cloud-only).

Table 1. MODIS Terra Granules Used in the Analysis, Location and Mean Solar Zenith Angle (SZA) Near the Data Granule Center, the Liquid Phase Cloud Fraction (CF), the Mean Optical Thickness and Effective Particle Radius of the Liquid Phase Clouds, and the Mean Broadband Surface Albedo

Date	Time (UTC)	Approximate Location	Mean SZA	Liquid CF (%)	Mean τ	Mean r_e (μm)	Mean Surface Albedo
4 Oct 2005	1550	13°S, 83°W	23.6°	75.7	11.6	14.6	0.051
26 Jan 2005	0745	20°N, 44°E	45.8°	17.1	11.9	10.1	0.172

the National Center for Environmental Prediction (NCEP) Global Data Assimilation System (GDAS) product [*Derber et al.*, 1991]. This data set is identical to the one used in the operational MODIS retrievals. The product also provides total (column) ozone concentration. The CO_2 concentration is set at 370 ppm. The cloud is placed in the layer whose top temperature is closest to the retrieved cloud top temperature. While cloud vertical location is only crudely resolved in our coarse vertical grid, additional refinements are not justified considering the nature of susceptibility calculations (differences between shortwave flux calculations).

[39] Figures 8a and 8b show liquid phase cloud optical thickness, effective radius, and absolute and relative susceptibility fields of albedo and absorptance for the two example granules. Susceptibilities were calculated using the SZA information in the Level 2 product. Correlations between the effective radius and the absolute susceptibility fields, and between the optical thickness and the relative susceptibility fields, follow predictions from the theoretical results shown in the previous section. Consistent with Figures 1 and 2, S^{rel} is in general greater than S given the magnitude of $\Delta N/N$ and ΔN perturbations and the fact that values of $r_e < 15$ μm and moderate optical thicknesses dominate both granules. The exception is the broken cloud portion of the 1550 UTC granule (coastal Peru) where high effective radii (red color indicates $r_e \sim 20$ μm and higher) raise the values of S above 8 mm^3. These large r_e may be related, in part, to 3-D radiative effects in the broken cloud fields. While such 3-D-related biases have been demonstrated in MODIS retrievals using high spatial resolution Advanced Spaceborne Thermal Emission and Reflection Radiometer (ASTER) imagery [*Marshak et al.*, 2006], the same study showed that large r_e can occur in portions of a boundary layer cloud field without being associated with an apparent 3-D cloud structure. The possibility of large r_e associated with drizzle is another possible explanation for some of these retrievals [e.g., *Wood*, 2000]. The S values for the 0745 UTC granule (Arabian Peninsula) are consistently lower than for the coastal Peru granule for four main reasons: (1) the smaller population of pixels with large r_e values, (2) the larger population of pixels with optical thicknesses greater than those giving susceptibility maxima, (3) larger surface albedos, and (4) larger SZA. The impact of surface albedo can be seen in the Arabian Peninsula granule image by contrasting portions of the cloudy field above land and ocean with similar τ and r_e. Differences in the structure of the absolute and relative absorptance susceptibility fields can be seen for both scenes. With regards to absolute absorptance susceptibility, large areas of both granules are covered by values very close to zero, while positive values of relative absorptance susceptibility dominate in the coastal Peru granule and negative values

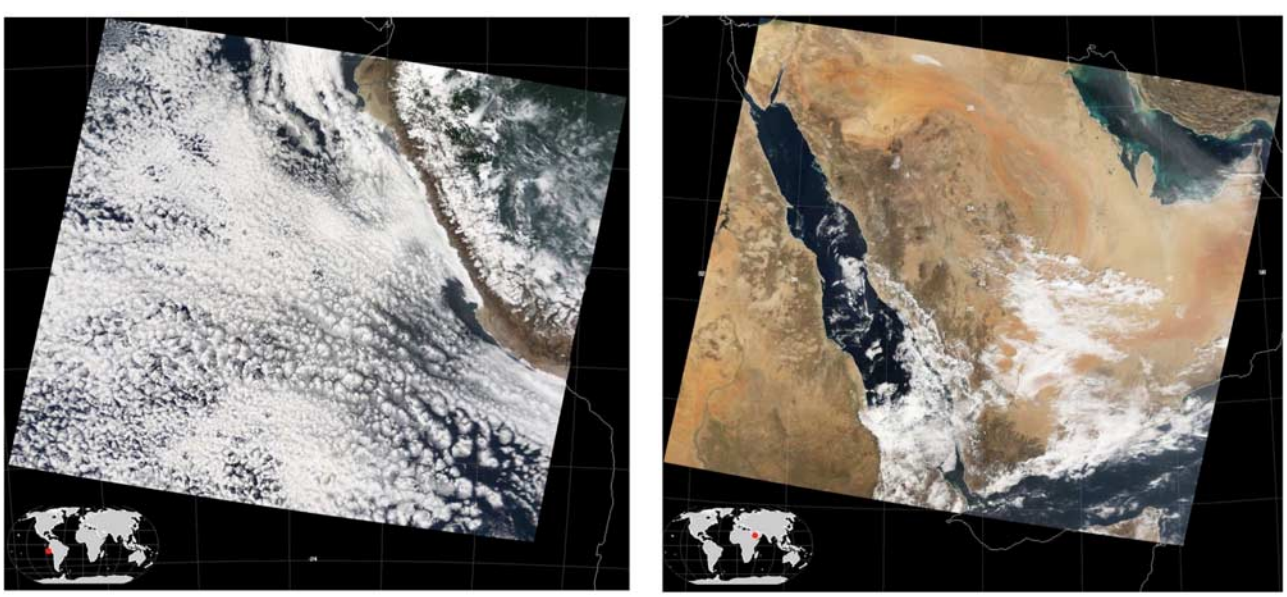

Figure 7. RGB true color composites for the two MODIS Terra Joint Product data granules analyzed in this study. (left) 4 October 2005, 1550 UTC, centered off coastal Peru, and (right) 26 January 2005, 0745 UTC, centered over the Arabian Peninsula (see also Table 1).

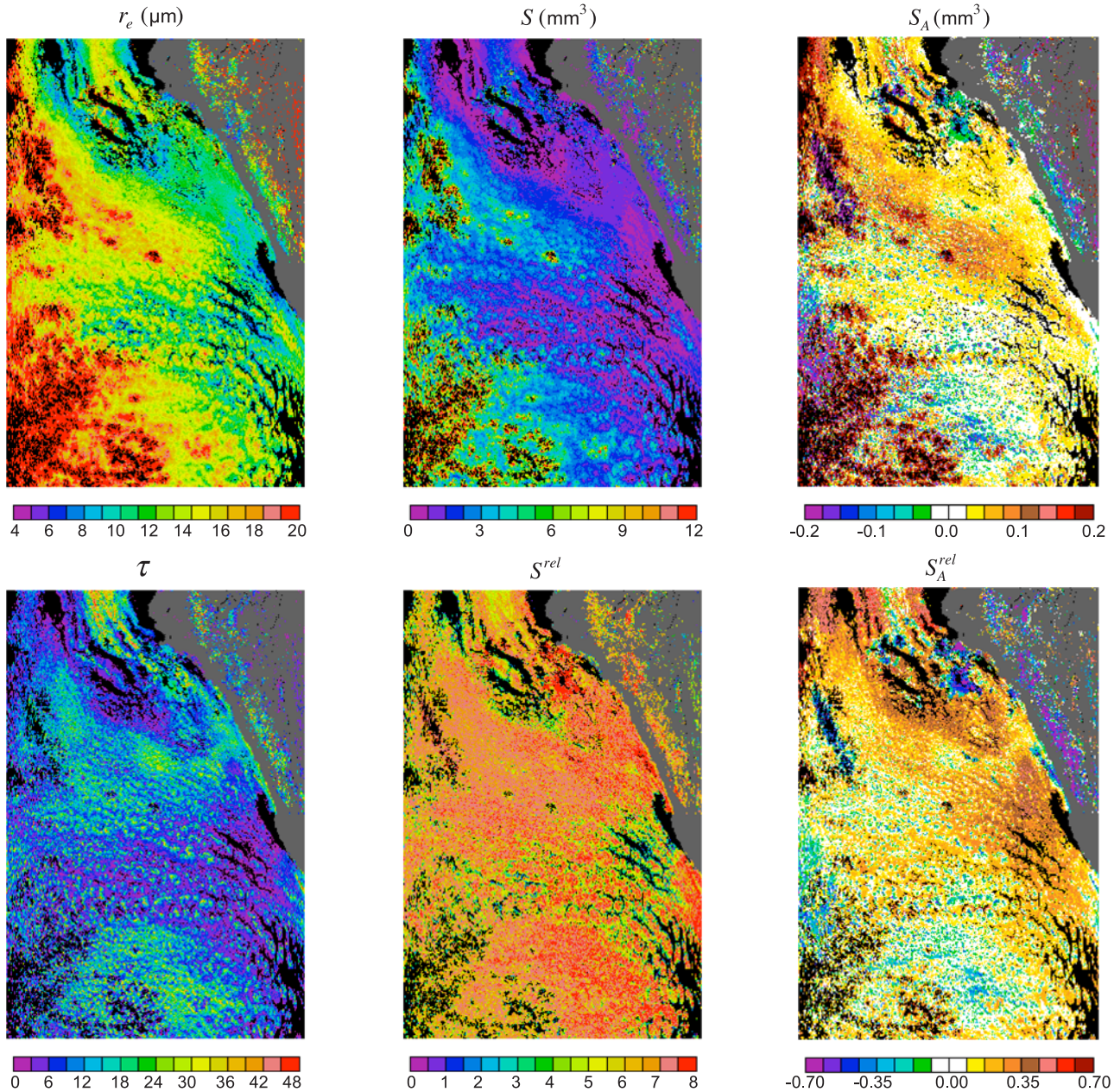

Figure 8a. Fields of cloud optical thickness, effective radius, absolute albedo, and absorptance susceptibility ($\Delta N = 1$ cm^{-3}, $w = 0.3$ gm^{-3}) and relative albedo and absorptance susceptibility ($\Delta N/N =$ 10%) for the liquid water portion of the coastal Peru MODIS data granule. Atmospheric and surface albedo effects are accounted for in the susceptibility calculations. Relative susceptibilities have been multiplied by 1000.

dominate in the Arabian Peninsula granule. While this general observation is consistent with the behavior of S_A^{rel} in Figure 2 and the higher values of τ for the Arabian Peninsula, a more consistent interpretation with Figure 2 cannot be achieved because of the different observation conditions (SZA, atmospheric and surface effects).

[40] The pixel-level susceptibilities and their relationship to various cloud properties can be seen more clearly in the scatterplots of Figure 9 that are derived from the coastal Peru granule data. As expected, albedo and optical thickness correlations with relative susceptibility are quite pronounced, but there is no apparent correlation with effective radius. This is in contrast to absolute susceptibility, which is highly correlated with effective radius.

[41] The coastal Peru granule data are also used to assess the contribution of $\Delta\omega$ and Δg perturbations to the total (or all-term) susceptibility in the presence of atmospheric and surface (albeit modest albedo) effects. For the distribution of optical properties observed within this particular granule, the two minor susceptibility terms add on average 15 to 17% to the one-term susceptibility (Figure 10). Referring back to Figure 1, note that the magnitude of the Δr_e perturbations for these granules have a much wider range

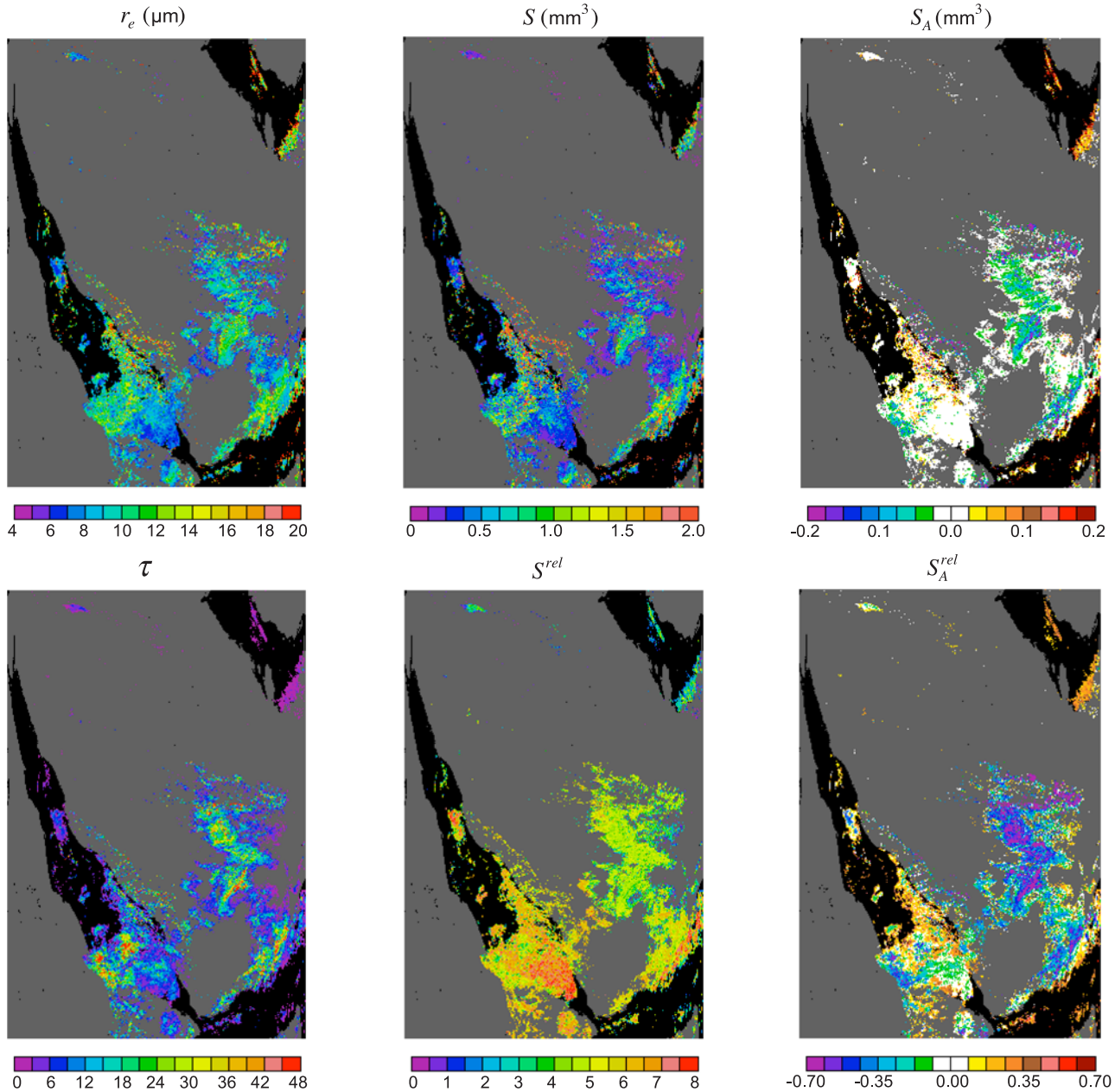

Figure 8b. As in Figures 8a but for the Arabian Peninsula MODIS data granule.

for absolute susceptibility calculations than for relative susceptibility.

6. Discussion and Conclusions

[42] Theoretical and observation-based approaches to examining potential broadband radiative changes in atmospheric column albedo, transmittance, and absorptance due to prescribed changes in liquid water cloud droplet number concentration (N) for a constant water path and water content process have been presented. Two types of droplet perturbations were considered: absolute increases, the radiative response to which we refer to as absolute cloud susceptibility, and relative increases, referred to as relative cloud susceptibility. Estimation of the former is more challenging as it requires an assumed value for either cloud liquid water content or geometrical thickness; a relationship between droplet volume radius and effective radius is needed for both (e.g., parameter k) and is assumed fixed while the droplet concentration is perturbed. A GCM-type broadband shortwave radiative transfer model is used to produce the radiative fluxes for the unperturbed and perturbed cloud; the normalized (by the incident flux) difference of these two calculations gives cloud susceptibility. Droplet perturbations of $\Delta N = 1$ cm^{-3} and $\Delta N/N = 10\%$ for absolute and relative susceptibility, respectively, were used in most calculations. These droplet concentration perturbations are understood to represent just one subset of potential changes due to the infusion of additional CCN particles into a cloud with constant liquid water path, and are intended as examples useful for understanding susceptibility magni-

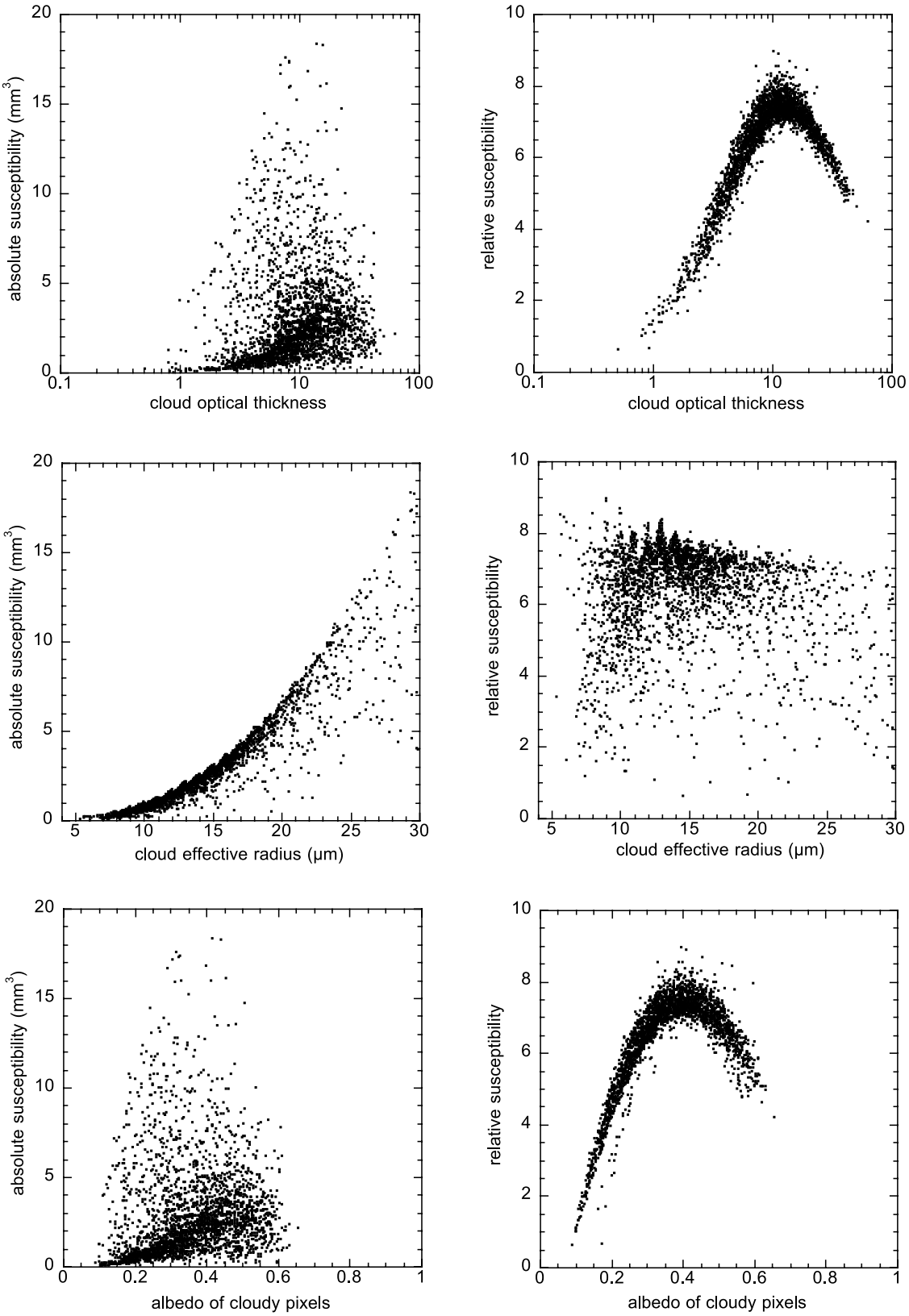

Figure 9. Dependence of (left) absolute (ΔN = 1 cm^{-3}, w = 0.3 gm^{-3}) and (right) relative ($\Delta N/N$ = 10%) albedo susceptibility on cloud optical thickness, effective radius, and cloud albedo for the coastal Peru MODIS data granule. Relative susceptibilities have been multiplied by 1000.

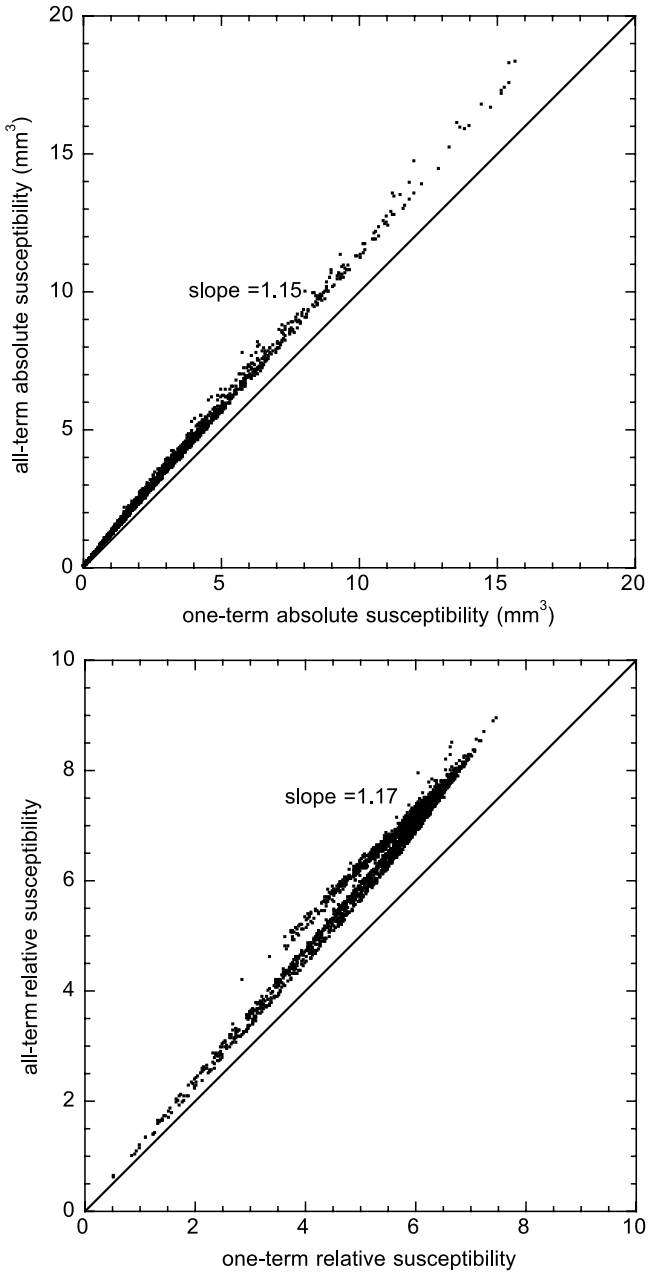

Figure 10. Pixel-level scatterplot of all-term versus one-term cloud albedo susceptibility for (top) $\Delta N = 1$ cm^{-3} ($w = 0.3$ gm^{-3}) and (bottom) $\Delta N/N = 10\%$ perturbations for the coastal Peru MODIS data granule (atmospheric and surface effects included). Relative susceptibilities have been multiplied by 1000.

tudes and dependencies on cloud, atmosphere, and surface properties.

[43] Absolute susceptibilities (albedo, transmittance, and absorptance) have a strong dependence on the droplet effective radius of the unperturbed cloud, while relative cloud susceptibilities are more sensitive to the optical thickness. For a given effective radius, absolute and relative albedo susceptibilities peak at values of optical thickness ~5–10 with considerable sensitivity to the solar geometry. For accurate broadband calculations of cloud susceptibility, the impact of effective radius perturbations on optical properties other than the extinction coefficient (i.e., single-scattering albedo and asymmetry parameter) must be included. When this is not done, a 10–30% underestimation in susceptibility can easily result for typical water clouds. Above-cloud molecular (or aerosol) absorption/scattering and a reflective surface lower the albedo susceptibility because the relative contribution of the cloud to the total atmospheric column albedo is reduced.

[44] For optically thin water clouds with moderate to large effective radii over a black surface, the absolute magnitude of albedo susceptibility (absolute and relative) is slightly smaller than that of transmittance susceptibility giving rise to positive atmospheric absorptance susceptibilities in that region of the τ, r_e space. Otherwise, the absolute magnitude of susceptibility for albedo is slightly larger than for transmittance giving rise to negative absorptance susceptibilities. Both absolute and relative absorptance susceptibilities are about an order of magnitude smaller than for albedo or transmittance.

[45] Our observationally driven calculations are based on two data granules of MODIS Terra retrievals of liquid cloud optical thickness and effective radius at ~1 km scales subsampled at ~5 km. These calculations offer the opportunity to examine the validity of the theoretically derived dependencies in the presence of realistic atmospheric and surface conditions and for the portion of τ, r_e space that is most often encountered.

[46] The concept of susceptibility provides a framework for identifying liquid water cloud types and geographic regions that will have the strongest radiative response to changes in microphysical properties. Though our susceptibility study does not attempt to link radiative responses to particular aerosol perturbation scenarios, it is directly relevant to the 1st IAE. Susceptibility allows for observation-based global estimates of the 1st IAE for a range of cloud perturbation scenarios (see Part 2) and provides additional constraints on cloud properties used in indirect effect modeling studies. Susceptibility also provides a means for analyzing indirect effect uncertainties in a self-consistent manner. This is because such uncertainties belong to one of three categories: (1) uncertainties in the absolute or relative changes in droplet number concentration, (2) uncertainties in the microphysical and optical properties of the unperturbed clouds, and (3) uncertainties in the state of the atmosphere and surface. The present work (including Part 2) is intended to provide impetus for progress in understanding and quantifying the role of these uncertainties.

[47] **Acknowledgments.** Warm memories of Yoram Kaufman and our many interactions with him accompanied the writing of this paper. We thank Eric Moody for software to read and interpolate the MODIS surface albedo product, Gala Wind for software to read the GDAS atmospheric profiles, and G. Thomas Arnold for the code that generated the color plots for the two MODIS scenes used in this study. We are grateful for comments from Graham Feingold, Paquita Zuidema, and an anonymous reviewer. Both authors wish to acknowledge support from the NASA Radiation Science Program. L. Oreopoulos also gratefully acknowledges support from the U.S. Department of Energy, Office of Science, Office of Biological and Environmental Research, Environmental Sciences Division as part of the ARM program under grant DE-FG02-07ER64354.

References

Ackerman, A. S., O. B. Toon, J. P. Taylor, D. W. Johnson, P. V. Hobbs, and R. J. Ferek (2000), Effects of aerosols on cloud albedo: Evaluation of

Twomey's parameterization of cloud susceptibility using measurements of ship tracks, *J. Atmos. Sci.*, *57*, 2684–2695, doi:10.1175/1520-0469(2000)057<2684:EOAOCA>2.0.CO;2.

Ackerman, A. S., M. P. Kirkpatrick, D. E. Stevens, and O. B. Toon (2004), The impact of humidity above stratiform clouds on indirect aerosol climate forcing, *Nature*, *432*, 1014–1017, doi:10.1038/nature03174.

Albrecht, B. A. (1989), Aerosols, cloud microphysics and fractional cloudiness, *Science*, *245*, 1227–1230, doi:10.1126/science.245.4923.1227.

Bennartz, R. (2007), Global assessment of marine boundary layer cloud droplet number concentration from satellite, *J. Geophys. Res.*, *112*, D02201, doi:10.1029/2006JD007547.

Brenguier, J. L., H. Pawlowska, L. Schüller, R. Preusker, J. Fischer, and Y. Fouquart (2000), Radiative properties of boundary layer clouds: Droplet effective radius versus number concentration, *J. Atmos. Sci.*, *57*, 803–821, doi:10.1175/1520-0469(2000)057<0803:RPOBLC>2.0.CO;2.

Chou, M.-D., and M. J. Suarez (2002), A solar radiation parameterization for atmospheric studies, *NASA Tech. Memo., NASA/TM-1999-10460,* vol. 15, 52 pp.

Chou, M.-D., M. J. Suarez, C.-H. Ho, M.-H. M.Yan, and K.-T. Lee (1998), Parameterizations for cloud overlapping and shortwave single-scattering properties for use in general circulation and cloud ensemble models, *J. Clim.*, *11*, 202–214, doi:10.1175/1520-0442(1998)011<0202:PFCOAS>2.0.CO;2.

Chuang, C. C., J. E. Penner, J. M. Prospero, K. E. Grant, G. H. Rau, and K. Kawamoto (2002), Cloud susceptibility and the first aerosol indirect forcing: Sensitivity to black carbon and aerosol concentrations, *J. Geophys. Res.*, *107*(D21), 4564, doi:10.1029/2000JD000215.

Derber, J. C., D. F. Parrish, and S. J. Lord (1991), The new global operational analysis system at the National Meteorological Center, *Weather Forecast.*, *6*, 538–547, doi:10.1175/1520-0434(1991)006<0538:TNGOAS>2.0.CO;2.

Feingold, G., and H. Seibert (2008), Cloud-aerosol interactions from the micro to the cloud scale, in *Frankfurt Institute for Advanced Studies Workshop: Perturbed Clouds in the Climate System*, MIT Press, Cambridge, Mass., in press.

Feingold, G., R. Boers, B. Stevens, and W. R. Cotton (1997), A modeling study of the effect of drizzle on cloud optical depth and susceptibility, *J. Geophys. Res.*, *102*, 13,527–13,534, doi:10.1029/97JD00963.

Hansen, J., M. Sato, A. Lacis, and R. Ruedy (1997), The missing climate forcing, *Philos. Trans. R. Soc. London, Ser. B*, *352*, 231–240, doi:10.1098/rstb.1997.0018.

Hu, Y. X., and K. Stamnes (1993), An accurate parameterization of the radiative properties of water clouds suitable for use in climate models, *J. Clim.*, *6*, 728–742, doi:10.1175/1520-0442(1993)006<0728:AAPOTR>2.0.CO;2.

Intergovernmental Panel on Climate Change (2007), *Climate Change 2007: The Physical Science Basis*, edited by S. Solomon, D. Qin, and M. Manning, Geneva, Switzerland. (Available at http://ipcc-wg1.ucar.edu/wg1/wg1-report.html)

Khain, A., D. Rosefeld, and A. Pokrovsky (2005), Aerosol impact on the dynamics and microphysics of convective clouds, *Q. J. R. Meteorol. Soc.*, *131*, 2639–2663, doi:10.1256/qj.04.62.

Koren, I., Y. J. Kaufman, L. A. Remer, and J. V. Martins (2004), Measurement of the effect of Amazon smoke on inhibition of cloud formation, *Science*, *303*, 1342–1345, doi:10.1126/science.1089424.

Marshak, A., S. Platnick, T. Várnai, G. Wen, and R. F. Cahalan (2006), Impact of three-dimensional radiative effects on satellite retrievals of cloud droplet sizes, *J. Geophys. Res.*, *111*, D09207, doi:10.1029/2005JD006686.

Martin, G. M., D. W. Johnson, and A. Spice (1994), The measurement and parameterization of effective radius of droplets in warm stratocumulus clouds, *J. Atmos. Sci.*, *51*, 1823–1842, doi:10.1175/1520-0469(1994)051<1823:TMAPOE>2.0.CO;2.

Matsui, T., H. Masunaga, S. M. Kreidenweis, R. A. Pielke Sr., W.-K. Tao, M. Chin, and Y. J. Kaufman (2006), Satellite- based assessment of marine low cloud variability associated with aerosol, atmospheric stability, and the diurnal cycle, *J. Geophys. Res.*, *111*, D17204, doi:10.1029/2005JD006097.

McFarquhar, G. M., and A. J. Heymsfield (2001), Parameterization of INDOEX microphysical measurements and calculations of cloud susceptibility: Applications for climate studies, *J. Geophys. Res.*, *106*, 28,675–28,698, doi:10.1029/2000JD900777.

Moody, E. G., M. D. King, S. Platnick, C. B. Schaaf, and F. Gao (2005), Spatially complete global spectral surface albedos: Value-added datasets derived from Terra MODIS land products, *IEEE Trans. Geosci. Remote Sens.*, *43*, 144–158, doi:10.1109/TGRS.2004.838359.

Nenes, A., R. J. Charlson, M. C. Facchini, M. Kulmala, A. Laaksonen, and J. H. Seinfeld (2002), Can chemical effects on cloud droplet number rival the first indirect effect?, *Geophys. Res. Lett.*, *29*(17), 1848, doi:10.1029/2002GL015295.

Oreopoulos, L., and S. Platnick (2008), Radiative susceptibility of cloudy atmospheres to droplet number perturbations: 2. Global analysis from MODIS, *J. Geophys. Res.*, *113*, D14S21, doi:10.1029/2007JD009655.

Pincus, R., and M. B. Baker (1994), Effect of precipitation on the albedo susceptibility of clouds in the marine boundary layer, *Nature*, *372*, 250–252, doi:10.1038/372250a0.

Platnick, S. (2000), Vertical photon transport in cloud remote sensing problems, *J. Geophys. Res.*, *105*(D18), 22,919–22,935.

Platnick, S., and S. Twomey (1994), Determining the susceptibility of cloud albedo to changes in droplet concentration with the Advanced Very High Resolution Radiometer, *J. Appl. Meteorol.*, *33*, 334–347, doi:10.1175/1520-0450(1994)033<0334:DTSOCA>2.0.CO;2.

Platnick, S., M. D. King, S. A. Ackerman, W. P. Menzel, B. A. Baum, J. C. Riedi, and R. A. Frey (2003), The MODIS cloud products: Algorithms and examples from Terra, *IEEE Trans. Geosci. Remote Sens.*, *41*, 459–473, doi:10.1109/TGRS.2002.808301.

Quaas, J., O. Boucher, and U. Lohmann (2006), Constraining the total aerosol indirect effect in the LMDZ and ECHAM4 GCMs using MODIS satellite data, *Atmos. Chem. Phys.*, *6*, 947–955.

Ramanathan, V., P. J. Crutzen, J. T. Kiehl, and D. Rosenfeld (2001), Aerosols, climate, and the hydrological cycle, *Science*, *294*, 2119–2124, doi:10.1126/science.1064034.

Ricchiazzi, P., S. Yang, C. Gautier, and D. Sowle (1998), SBDART: A research and teaching software tool for plane-parallel radiative transfer in the Earth's atmosphere, *Bull. Am. Meteorol. Soc.*, *79*, 2101–2114, doi:10.1175/1520-0477(1998)079<2101:SARATS>2.0.CO;2.

Sekiguchi, M., T. Nakajima, K. Suzuki, K. Kawamoto, A. Higurashi, D. Rosenfeld, I. Sano, and S. Mukai (2003), A study of the direct and indirect effects of aerosols using global satellite data sets of aerosol and cloud parameters, *J. Geophys. Res.*, *108*(D22), 4699, doi:10.1029/2002JD003359.

Taylor, J. P., and A. McHaffie (1994), Measurements of cloud susceptibility, *J. Atmos. Sci.*, *51*, 1298–1306, doi:10.1175/1520-0469(1994)051<1298:MOCS>2.0.CO;2.

Twomey, S. (1974), Pollution and the planetary albedo, *Atmos. Environ.*, *8*, 1251–1256, doi:10.1016/0004-6981(74)90004-3.

Twomey, S. (1991), Aerosols, clouds, and radiation, *Atmos. Environ.*, *254*, 2435–2442.

Wood, R. (2000), Parameterization of the effect of drizzle upon the droplet effective radius in stratocumulus clouds, *Q. J. R. Meteorol. Soc.*, *126*, 3309–3324, doi:10.1002/qj.49712657015.

Xue, H. W., and G. Feingold (2006), Large-eddy simulations of trade wind cumuli: Investigation of aerosol indirect effects, *J. Atmos. Sci.*, *63*, 1605–1622, doi:10.1175/JAS3706.1.

Zuidema, P., H. Xue, and G. Feingold (2008), Shortwave radiative impacts from aerosol effects on shallow marine cumuli, *J. Atmos. Sci.*, in press.

L. Oreopoulos, Joint Center for Earth Systems Technology, University of Maryland, Baltimore County, Baltimore, MD 21228, USA.

S. Platnick, Laboratory for Atmospheres, NASA Goddard Space Flight Center, Greenbelt, MD 20771, USA. (steven.platnick@nasa.gov)